JCI insight

RESEARCH ARTICLE

Endospanin-2 enhances skeletal muscle energy metabolism and running endurance capacity

Steve Lancel,[1,2,3,4] Matthijs K.C. Hesselink,[5] Estelle Woldt,[1,2,3,4] Yves Rouillé,[6] Emilie Dorchies,[1,2,3,4] Stephane Delhaye,[1,2,3,4] Christian Duhem,[1,2,3,4] Quentin Thorel,[1,2,3,4] Alicia Mayeuf-Louchart,[1,2,3,4] Benoit Pourcet,[1,2,3,4] Valérie Montel,[7] Gert Schaart,[5] Nicolas Beton,[8] Florence Picquet,[7] Olivier Briand,[1,2,3,4] Jean Pierre Salles,[8] Hélène Duez,[1,2,3,4] Patrick Schrauwen,[5] Bruno Bastide,[7] Bernard Bailleul,[1,2,3,4], Bart Staels,[1,2,3,4] and Yasmine Sebti[1,2,3,4]

[1]Université de Lille, U1011 - EGID, F-59000 Lille, France. [2]Inserm, U1011, F-59000 Lille, France. [3]CHU Lille, F-59000 Lille, France. [4]Institut Pasteur de Lille, F-59000 Lille, France. [5]School for Nutrition, Toxicology and Metabolism, Deptartments of Human Biology and Human Movement Sciences, Maastricht University Medical Center, NL-6200 MD Maastricht, the Netherlands. [6]Center of Infection and Immunity of Lille (CIIL), Inserm, U1019, CNRS UMR-8204, Institut Pasteur de Lille, Université de Lille, France. [7]URePSS, Université de Lille, EA 7369, F-59650 Villeneuve d'Ascq, France. [8]INSERM UMR1043 (CPTP), Université de Toulouse, Paul Sabatier, Hôpital des Enfants, CHU de Toulouse, Toulouse, France.

Metabolic stresses such as dietary energy restriction or physical activity exert beneficial metabolic effects. In the liver, endospanin-1 and endospanin-2 cooperatively modulate calorie restriction–mediated (CR-mediated) liver adaptations by controlling growth hormone sensitivity. Since we found CR to induce endospanin protein expression in skeletal muscle, we investigated their role in this tissue. In vivo and in vitro endospanin-2 triggers ERK phosphorylation in skeletal muscle through an autophagy-dependent pathway. Furthermore, endospanin-2, but not endospanin-1, overexpression decreases muscle mitochondrial ROS production, induces fast-to-slow fiber-type switch, increases skeletal muscle glycogen content, and improves glucose homeostasis, ultimately promoting running endurance capacity. In line, *endospanin-2*$^{-/-}$ mice display higher lipid peroxidation levels, increased mitochondrial ROS production under mitochondrial stress, decreased ERK phosphorylation, and reduced endurance capacity. In conclusion, our results identify endospanin-2 as a potentially novel player in skeletal muscle metabolism, plasticity, and function.

Introduction

Besides its role in locomotion, skeletal muscle also controls whole body energy metabolism and expenditure. Skeletal muscle is a highly plastic tissue composed of slow and fast fibers that exhibit different oxidative and glycolytic metabolic capacities adapting to environmental conditions such as nutrient availability and physical activity. The adaptations of skeletal muscle to physiological stimuli involve changes in mass, myofiber composition, and mitochondrial properties associated with appropriate metabolic modifications. Mitochondria not only produce energy necessary for myofiber contractions, but they are also major producers of ROS. Pathophysiological conditions, such as obesity, type 2 diabetes, and aging, have been associated with impaired skeletal muscle oxidative metabolism and increased ROS production (1, 2). Conversely, calorie restriction (CR) or exercise both protect from age-related pathologies, notably by decreasing skeletal muscle oxidative stress (3). Activation of autophagy, a key stress response pathway, is also implicated in the beneficial effects of exercise and CR, notably by preventing the accumulation of damaged cellular components (4–6).

Endospanin-1, also named Leptin receptor overlapping transcript (LEPROT), and endospanin-2, also named LEPROT-like 1 (LEPROTL1) (7, 8), belong to a gene family derived from a unique ancestor gene encoding vacuolar protein sorting 55 (VPS55) in *Saccharomyces cerevisiae* (9). The endospanins and VPS55 tetraspan membrane proteins are located in the trans-Golgi network and endosomes and participate in the intracellular trafficking of various proteins, such as cell surface receptors in mammals or vacuolar carboxypeptidase Y in yeast, to the vacuole/lysosome (9–12), suggesting a phylogenetically conserved role of

Authorship note: BB, BS, and YS are co–senior authors.

Conflict of interest: The authors have declared that no conflict of interest exists.

Submitted: October 13, 2017
Accepted: March 28, 2018
Published: May 3, 2018

Reference information:
JCI Insight. 2018;3(9):e98081. https://doi.org/10.1172/jci.insight.98081.

these proteins in protein trafficking. We have previously demonstrated that endospanin-1 and endospanin-2 cooperate to decrease cell-surface abundance of the growth hormone (GH) receptor in the liver in periods of reduced nutrient availability, therefore decreasing plasma IGF1 levels (12). Moreover, endospanin expression is induced in liver and chondrocytes during CR, mediating an FGF-21–dependent reduction in GH sensitivity (13). Altogether, these observations identify a key role for these proteins in CR-induced metabolic adaptations. Since we found CR to also induce their protein expression in skeletal muscle, we investigated their role in this tissue. Here, using both gain- and loss-of-function models, we demonstrate that endospanin-2, but not endospanin-1, triggers ERK phosphorylation in skeletal muscle through autophagy activation, which results in decreased oxidative stress, fast-to-slow fiber-type switch, and enhanced glucose metabolism and glycogen storage. Finally, we show that endospanin-2 overexpression promotes running endurance capacity, while endospanin-2 downregulation induced the opposite phenotype. These findings identify endospanin-2 as a critical regulator of skeletal muscle plasticity, function, and metabolic flexibility.

Results

CR induces endospanin expression in skeletal muscle. Since CR enhances endospanin expression in the liver and the tibial growth plate in mice (12, 13), we assessed total endospanin expression upon CR in skeletal muscle using antibodies targeting the conserved C-terminus of both endospanin-1 and -2. After 4 weeks of CR, endospanin protein levels increased in skeletal muscle of WT mice (Supplemental Figure 1A; supplemental material available online with this article; https://doi.org/10.1172/jci.insight.98081DS1), whereas their mRNA levels remained unchanged (Supplemental Figure 1B). In line, 4 weeks of CR also increased Tg endospanin-2 and endospanin-1 protein but not their mRNA levels in skeletal muscle of endospanin-1 and endospanin-2 Tg mice (Supplemental Figure 1, C–F). These results indicate that CR upregulates endospanin protein expression through posttranslational mechanisms.

Endospanin-2 decreases mitochondrial oxidative stress. Given the role of CR to preserve skeletal muscle from oxidative damage by decreasing mitochondrial superoxide emission and increasing antioxidant defences (3, 14), we assessed whether overexpression of endospanins modulate oxidative stress levels. H_2O_2 plasma levels were 20% lower in endospanin-2 Tg, but not in endospanin-1 Tg mice, when compared with WT littermates (Figure 1A). Since other biochemical and functional parameters (data not shown) were also unchanged in endospanin-1 Tg compared with WT littermate mice, we further focused on endospanin-2 Tg mice only. In line with the decrease of plasma H_2O_2, levels of malondialdehyde (MDA), a marker of lipid peroxidation, were 50% lower in glycolytic muscles from endospanin-2 Tg compared with WT mice (Figure 1B). To determine whether mitochondria are implicated in this oxidative stress reduction, ROS production was measured in isolated mitochondria incubated under stress conditions. Succinate-driven ROS production through reverse electron flow from complex II to complex I was 65% lower in skeletal muscle mitochondria of endospanin-2 Tg mice (Figure 1C). Moreover, complex III ROS production measured after addition of the respective complex I and III chain inhibitors, rotenone, and antimycin A was 60% lower in glycolytic muscle mitochondria from endospanin-2 Tg compared with WT mice (Figure 1C). In addition, endospanin-2 Tg glycolytic muscle exhibited a 2.8-fold higher catalase activity (Figure 1D). To study whether endospanin-2 regulates mitochondrial ROS production in a cell-autonomous manner, C2C12 muscle cells were stably infected with endospanin-1 or endospanin-2 coding retroviruses. In line with the in vivo results, intracellular H_2O_2 levels measured using 2',7'-dichlorofluorescein diacetate (DCF-DA), a hydrogen peroxide–sensitive fluorescent probe, revealed significantly lower (~30%) ROS production in C2C12 myotubes overexpressing endospanin-2, but not endospanin-1, compared with control infected cells (Figure 1E). To confirm that endospanin-2 directly modulates mitochondrial superoxide generation, experiments were performed using MitoSox, a superoxide-specific probe selectively targeted to mitochondria (15). While antimycin A–driven mitochondrial superoxide production was markedly lower in C2C12 myotubes overexpressing endospanin-2 (Figure 1F), endospanin-2 silencing increased antimycin A–stimulated superoxide production (Figure 1G). These mitochondrial ROS production modifications were not related to changes in mitochondrial mass or respiration (Supplemental Figure 2). Interestingly, mRNA and protein expression of UCP3 were lower in endospanin-2 Tg glycolytic muscle (Supplemental Figure 3A) and in endospanin-2–overexpressing C2C12 cells (Supplemental Figure 3B), likely reflecting an adaptive response to reduced mitochondrial ROS production.

Altogether, these data indicate that endospanin-2 regulates skeletal muscle mitochondrial ROS production.

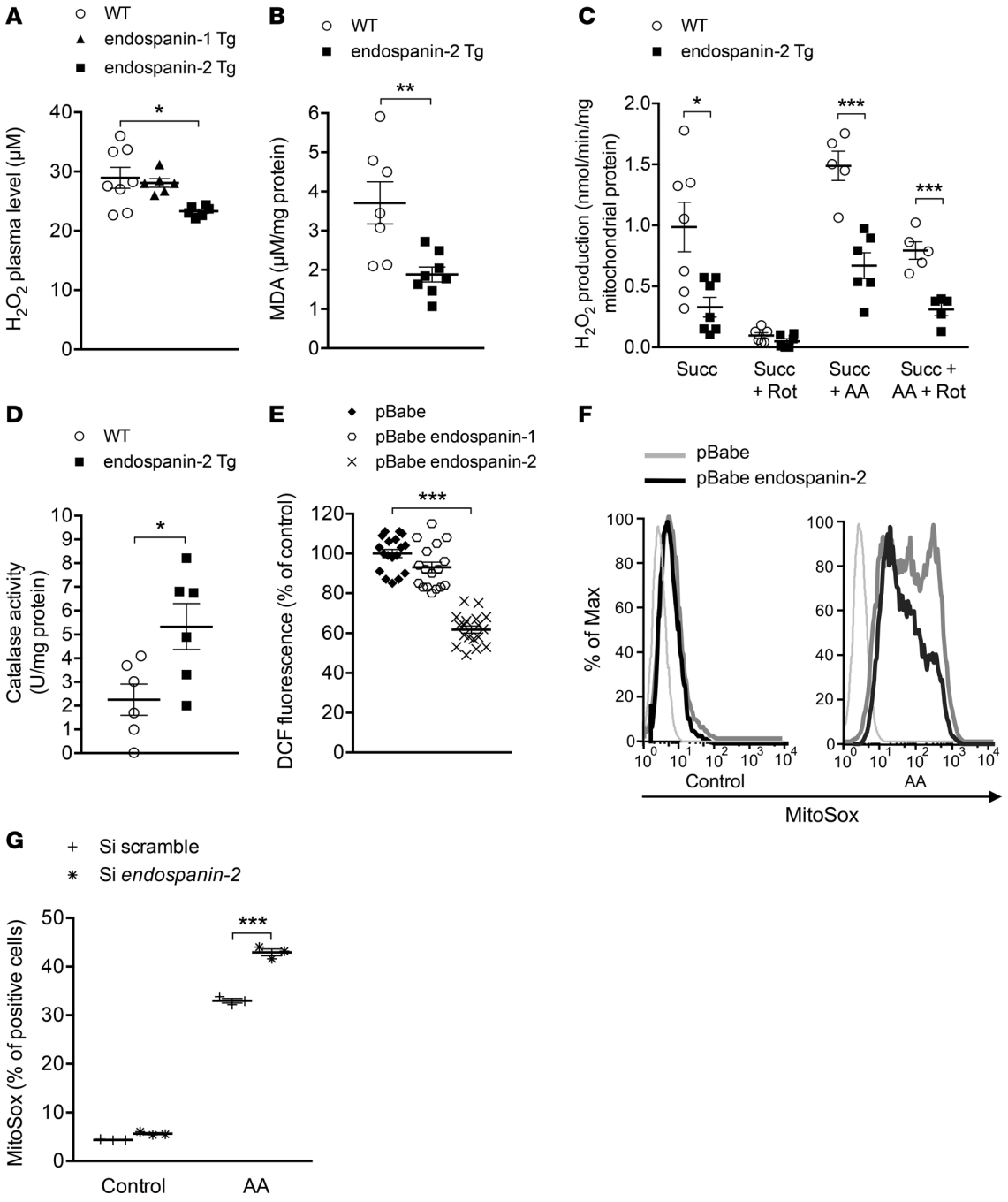

Figure 1. Endospanin-2, but not endospanin-1, decreases mitochondrial oxidative stress in vivo and in vitro. (**A**) Plasma H_2O_2 levels of endospanin-1 Tg mice, endospanin-2 Tg mice, and their WT littermates (n = 7–8 per genotype). (**B**) Malondialdehyde (MDA) levels in quadriceps from endospanin-2 Tg mice and their WT littermates (n = 7–8 per genotype). (**C**) Mitochondrial H_2O_2 production measured on isolated mitochondria and expressed per mg of mitochondrial protein. Mitochondrial substrates and inhibitors were sequentially added: 10 mM succinate (Succ), 1 μM rotenone (Rot), 2.5 μM antimycin A (AA). All experiments were done on quadriceps from endospanin-2 Tg mice and their WT littermates (n = 6 per genotype). (**D**) Catalase activity in quadriceps from endospanin-2 Tg mice and their WT littermates (n = 6 per genotype). (**E**) Intracellular ROS analysis using 2',7'-dichlorofluorescein diacetate (DCF-DA) on differentiated endospanin-1, endospanin-2, or control pBabe C2C12 cells (n = 6 per condition). (**F**) Representative histograms of flow cytometry experiments, using superoxide-specific probe MitoSox, illustrating the increase in mean fluorescence intensity and percentage of positive cells following AA pretreatment on differentiated endospanin-2 or control (pBabe) retrovirus-infected C2C12 cells. (**G**) C2C12 were transfected with control and *endospanin-2* siRNAs (mRNA levels decreased by 85%), and percentage of positive cells for MitoSOX was evaluated by flow cytometry in absence or presence of AA (n = 6 per condition). Results are expressed as means ± SEM and were analyzed by unpaired t test, except for **E**, which was analyzed by 1-way ANOVA. $^*P < 0.05$, $^{**}P < 0.01$, and $^{***}P < 0.001$.

Endospanin-2 activates the ERK pathway. The ERK pathway is involved in survival processes in response to cellular stresses and also plays an important role in the regulation of mitochondrial function (16, 17). Since, ERK stimulates Stat3 translocation to mitochondria by enhancing Stat3 phosphorylation on Serine 727, hence downregulating ROS production (18–20), we next assessed ERK phosphorylation levels in endospanin-2 Tg muscles. Interestingly, basal ERK1/2 phosphorylation levels were higher in endospanin-2 Tg mice (Figure 2A), associated with higher Ser 727 Stat3 phosphorylation (Figure 2B). Moreover, p-ERK, total ERK, and Stat3 were more abundant in purified skeletal muscle mitochondria from endospanin-2 Tg compared with WT littermate mice (Figure 2C and Supplemental Figure 4A). Mitochondrial ERK localization and activity have been associated with mitochondrial permeability transition pore (mPTP) opening desensitization under stress conditions (21). Interestingly, endospanin-2 overexpression increased the resistance to mPTP opening of isolated skeletal muscle mitochondria, demonstrating higher resistance to cellular stress (Figure 2D). ERK phosphorylation was also upregulated in endospanin-2–overexpressing C2C12 cells (Figure 2E). In line with these results, the protection from antimycin A–induced superoxide production observed in endospanin-2–overexpressing C2C12 cells was abolished by the addition of U0126, an inhibitor of ERK phosphorylation (Figure 2F and Supplemental Figure 4B), suggesting that ERK signaling participates in the endospanin-2–induced decrease of oxidative stress. Together, these data indicate that endospanin-2 regulates mitochondrial ROS production through activation of the ERK pathway.

To determine whether *endospanin-2* deficiency leads to a mirror phenotype, *endospanin-2*$^{-/-}$ mice were generated (Supplemental Figure 5, A and B). Opposite to endospanin-2 Tg mice, *endospanin-2*$^{-/-}$ mice displayed higher lipid peroxidation levels (Figure 3A) and increased mitochondrial ROS production under mitochondrial stress conditions (Figure 3B). Consistently, the ERK phosphorylation level was lower in *endospanin-2*$^{-/-}$ skeletal muscle (Figure 3C). By contrast, AAV-mediated skeletal muscle–specific endospanin-2 overexpression in vivo (Supplemental Figure 5C) resulted in a significant decrease in mitochondrial ROS production (Figure 3D) associated with higher basal ERK phosphorylation levels in skeletal muscle (Figure 3E). Altogether, these results demonstrate that skeletal muscle endospanin-2 activates the ERK pathway and regulates mitochondrial ROS production.

Endospanin-2 triggers ERK phosphorylation through autophagy activation. Endospanin-2 Tg mice displayed reduced skeletal muscle mass of the predominant glycolytic muscles (i.e., *extensor digitorum longus* [EDL], quadriceps, and gastrocnemius) compared with WT mice (Figure 4A). Interestingly, this reduction in muscle mass is associated with autophagy activation, a highly conserved cell survival process, linked to dietary restriction and exercise-conveyed skeletal muscle adaptations (22, 23). Indeed, protein levels of Ulk1, Atg5, Beclin, and the LC3-II/I ratio were increased in glycolytic muscles of endospanin-2 Tg mice (Figure 4B and Supplemental Figure 6A). The increase in autophagy was confirmed in vivo by electron microscopy analysis, revealing autophagosome structures in endospanin-2 Tg mouse glycolytic muscles (Figure 4C). By contrast, autophagy markers were not increased in the oxidative soleus muscle of endospanin-2 Tg mice compared with WT mice (Supplemental Figure 6B).

During autophagy, cytoplasmic material and organelles are sequestered within autophagosomes to be delivered to lysosomes for degradation. Since Vps55, the yeast endospanin homologue, promotes targeting of endocytosed proteins to the vacuole/lysosome (9), a key organelle in macroautophagy, we investigated whether cellular endospanin-2 is colocalized with autophagosomes upon modulation of autophagy. In basal conditions, endospanin-2 localized around the nucleus (Figure 4D and Supplemental Figure 6C), likely in the endosomal compartment (11). Interestingly, starvation of endospanin-2–overexpressing C2C12 cells — followed by treatment with chloroquine, a lysosomal inhibitor inducing accumulation of LC3-II–positive autophagosomes — resulted in endospanin-2 colocalization with LC3-II and the lysosome (Figure 4D and Supplemental Figure 6C). These results indicate that endospanin-2 traffics with autophagic structures to the lysosome upon autophagy activation.

Interestingly, autophagy has been recently shown to promote ERK phosphorylation (24). To determine whether endospanin-2 increases ERK phosphorylation through autophagy activation, C2C12 myotubes overexpressing endospanin-2 and control cells were treated with either the PI3K inhibitors wortmannin or chloroquine, which inhibit the autophagy process at early and late stages, respectively. In line with previous observations (24), blocking autophagosome formation by wortmannin decreased ERK phosphorylation, while chloroquine-induced autophagosome accumulation promoted ERK phosphorylation (Figure 4E). More importantly, the difference in ERK phosphorylation observed between endospanin-2–overexpressing and control C2C12 cells was abolished upon inhibition of autophagy by wortmannin and chloroquine (Figure 4E).

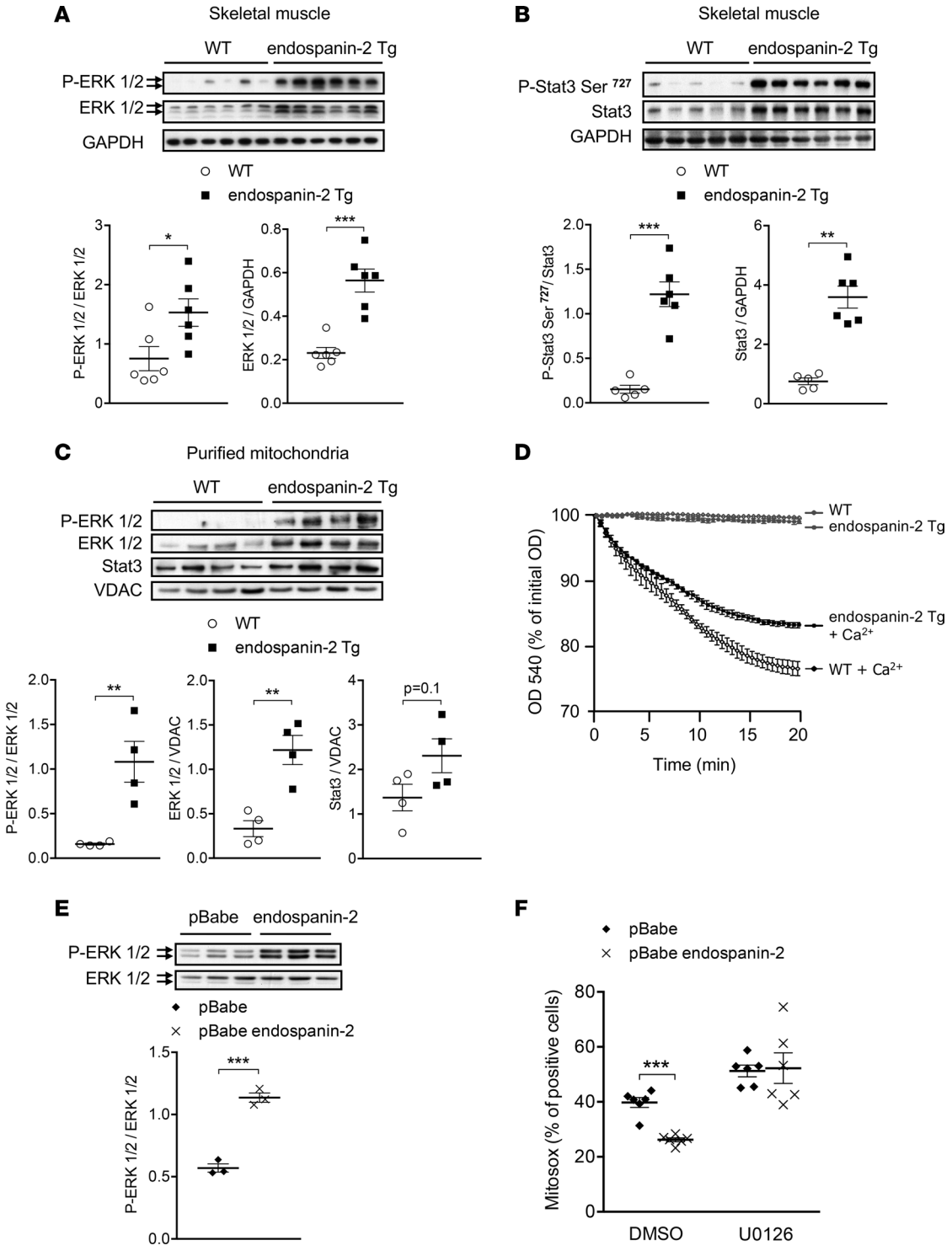

Figure 2. Endospanin-2 activates the ERK cellular stress pathway. Western blot analysis of (**A**) phosphorylated ERK 1/2, total ERK1/2, and (**B**) phosphorylated Stat3 on serine 727 residue and total stat3 protein levels in quadriceps from endospanin-2 Tg mice and their WT littermates (n = 6 per genotype). (**C**) Western blot analysis of phosphorylated ERK1/2, total ERK1/2, and total Stat3 protein levels on purified mitochondria (see extended experimental procedures and Supplemental Figure 4A) from endospanin-2 Tg mice and their WT littermates (n = 4 per genotype). (**D**) mPTP opening sensitivity assessed by monitoring OD 540 nm after 75 μM Ca^{2+} pulse on isolated mitochondria from endospanin-2 Tg mice and their WT littermates (n = 6 per genotype). (**E**) Western blot analysis of phosphorylated ERK 1/2 and total ERK1/2 protein levels on differentiated endospanin-2 or control (pBabe) retrovirus–infected C2C12 cells (n = 3 per condition). (**F**) Percentage of positive cells for MitoSOX ± antimycin A evaluated by flow cytometry on differentiated cells treated or not with U0126, an inhibitor of ERK phosphorylation (n = 5 per condition). Results are expressed as means ± SEM; $^*P < 0.05$, $^{**}P < 0.01$, and $^{***}P < 0.001$ by unpaired t test.

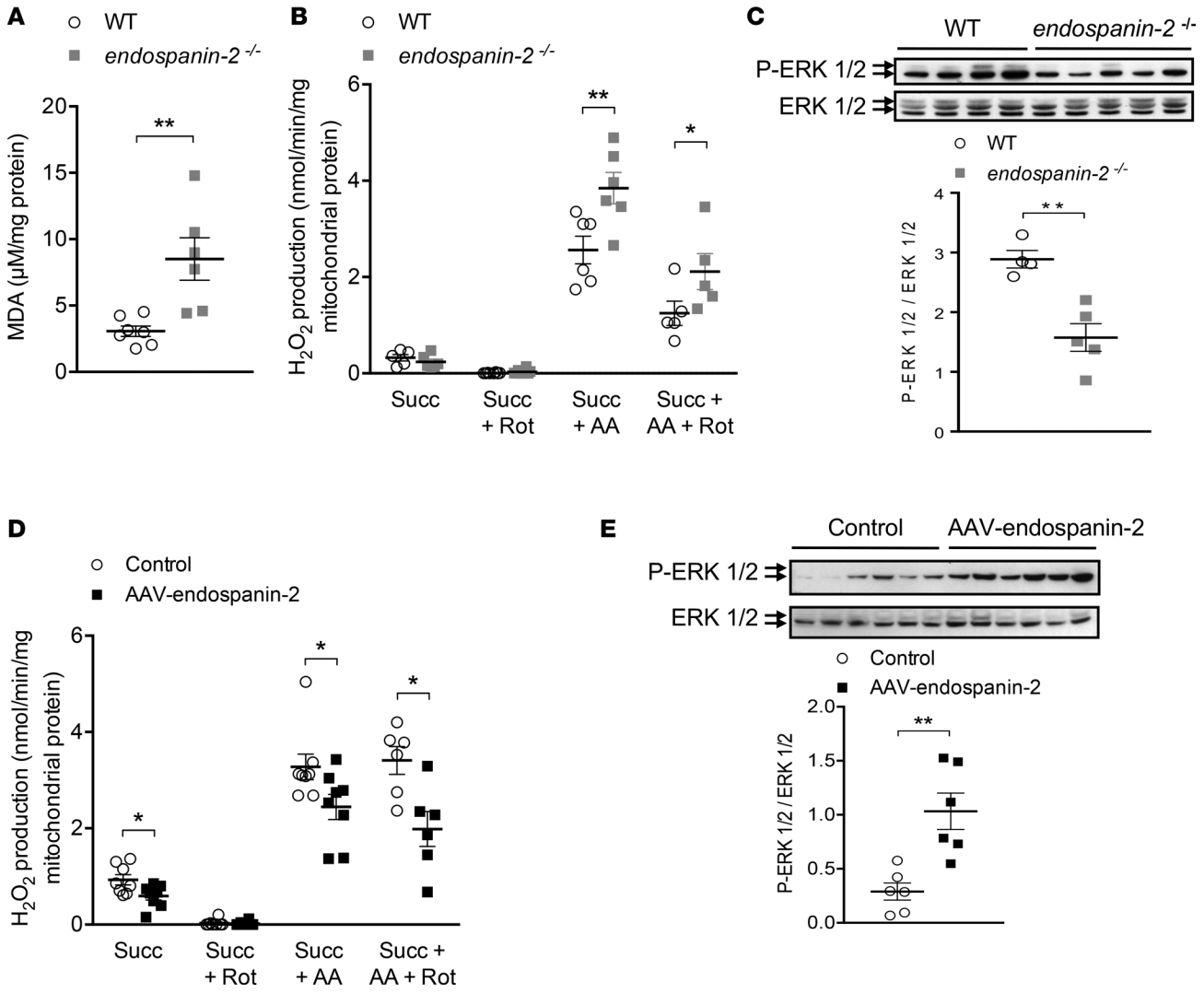

Figure 3. *Endospanin-2*$^{-/-}$ mice display increased oxidative stress and decreased ERK phosphorylation. (**A**) Skeletal muscle MDA levels in *Endospanin-2*$^{-/-}$ mice and their WT littermates (n = 6–8 per genotype). (**B**) Mitochondrial H_2O_2 production evaluated on isolated quadriceps muscle mitochondria from *endospanin-2*$^{-/-}$ and their WT littermates (n = 6–7 per genotype). (**C**) Western blot analysis of phosphorylated ERK 1/2 and total ERK 1/2 protein levels in the quadriceps from *endospanin-2*$^{-/-}$ mice and their WT littermates (n = 4–5 per genotype). (**D**) Mitochondrial H_2O_2 production evaluated on mitochondria isolated from gastrocnemius muscle from mice intramuscularly injected with an endospanin-2–expressing or a control AAV vector and treated with mitochondrial substrates and inhibitors (10 mM succinate [Succ], 1 μM rotenone [Rot], 2.5 μM antimycin A [AA]) (n = 8–10 per group). (**E**) Western blot analysis of phosphorylated ERK1/2 and total ERK1/2 protein levels in gastrocnemius from mice intramuscularly injected with an endospanin-2–expressing or a control AAV vector (n = 6 per group). Results are expressed as means ± SEM; *P < 0.05, **P < 0.01 by unpaired t test.

These data indicate that endospanin-2 regulates ERK phosphorylation through autophagy modulation.

Endospanin-2 regulates skeletal muscle plasticity and function. Considering that oxidative stress level, autophagy activation, and the ERK pathway regulate skeletal muscle plasticity and function (25–27), immunofluorescence analysis of the myosin heavy chain (MHC) isoforms was performed on EDL sections of endospanin-2 Tg and WT littermate mice. EDL from endospanin-2 Tg mice exhibited a lower proportion of glycolytic MHC2b and a higher proportion of MHC2x fibers compared with muscles from WT mice (Figure 5A). Moreover, the fiber-type switch was observed at both the mRNA and protein levels (Supplemental Figure 7, A and B). Although the total fiber number remained unchanged (Supplemental Figure 7C), the MHC2b fiber cross-section area (CSA) was significantly lower, while the MHC2x and hybrid fiber CSA was higher in EDL of endospanin-2 Tg compared with WT mice (Figure 5B). This fiber-type switch was not observed in the soleus oxidative muscle of endospanin-2 Tg compared with WT mice (Supplemental Figure 7D). Moreover, skeletal muscle fiber type and mass were not yet modified in young endospanin-2

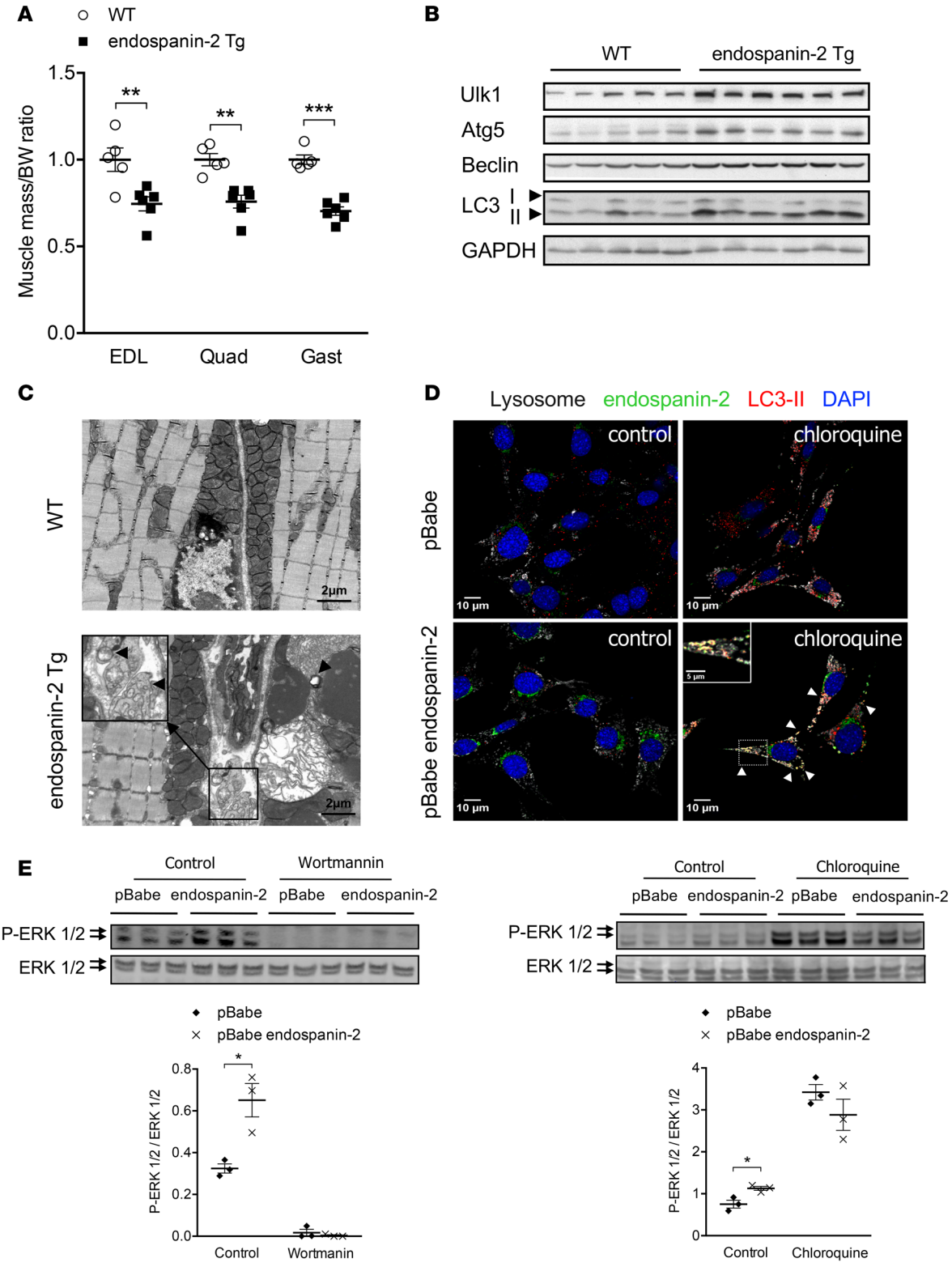

Figure 4. Endospanin-2 regulates ERK pathway through autophagy activation. (**A**) Muscle mass relative to body weight of endospanin-2 Tg mice and their WT littermates (n = 6 per genotype). (**B**) Western blot analysis of Ulk1, Atg5, Beclin, and LC3-I and LC3-II proteins levels in EDL muscle from endospanin-2 Tg mice compared with WT littermates (n = 5–6/genotype). (**C**) Representative images of electron microscopy analysis on EDL sections from endospanin-2 Tg mice compared with their WT littermate (n = 5–6 per genotype). Black arrowheads represent autophagosomal structures. (**D**) Representative images of immunofluorescence staining depicting colocalisation of lysosome (gray), LC3-II (red), and endospanin-2 (green) in endospanin-2–overexpressing C2C12 treated with chloroquine (50 μM) compared with control cells (n = 3 per condition). (**E**) Western blot analysis of phosphorylated ERK 1/2 and total ERK1/2 protein levels in endospanin-2 or control (pBabe) retrovirus-infected C2C12 cells cultured in nutrient-free medium (HBSS) treated with chloroquine (50μM), wortmannin (100 nM), or their respective vehicle for 4 hours (n = 3 per condition). Results are expressed as means ± SEM; $^{*}P < 0.05$, $^{**}P < 0.01$, and $^{***}P < 0.001$ by unpaired t test.

Tg mice compared with WT and endospanin-1 Tg mice (Supplemental Figure 7, E and F), suggesting that the endospanin-2–induced skeletal muscle phenotype is unlikely to be established during development.

By contrast, glycolytic muscles of endospanin-1 Tg mice did not display any phenotype and displayed no modification in fiber-type composition (Supplemental Figure 7, A and B) or mass (data not shown) compared with WT mice.

To investigate whether the fiber-type transition in endospanin-2 Tg mice is associated with changes in skeletal muscle function, the fatigue index was evaluated on dissected EDL from endospanin-2 Tg and WT mice. Consistent with the fast-to-slow fiber type, ex vivo endospanin-2 Tg EDL muscle was significantly more resistant to fatigue than EDL from WT mice (Figure 5C). Since metabolic challenges also impact skeletal muscle metabolism, we measured skeletal muscle glycogen level, an easily mobilized source of glucose upon sudden energy needs. Periodic acid–Schiff (PAS) staining (Figure 5D and Supplemental Figure 8A) and biochemical measurement of glycogen (Supplemental Figure 8B) revealed a significantly higher glycogen content in glycolytic muscles of endospanin-2 Tg mice compared with WT littermates. Given these findings, we also assessed whether endospanin-2 overexpression affects glucose homeostasis. Despite no changes in plasma insulin level (Supplemental Figure 8C), fasting plasma glucose was lower in endospanin-2 Tg mice (Supplemental Figure 8D), and this was associated with improved glucose tolerance (Figure 5E and Supplemental Figure 8E). Moreover, insulin-stimulated p-Akt levels were more strongly induced in skeletal muscle of endospanin-2 Tg mice compared with WT mice, indicating that skeletal muscle of endospanin-2 Tg mice are more sensitive to insulin than WT mice (Figure 5F and Supplemental Figure 8F). By contrast, *endospanin-2* $^{-/-}$ mice did not display any difference in glucose homeostasis compared with their WT littermates (Supplemental Figure 8G).

Finally, when submitted to an endurance exercise test to exhaustion at 70% of maximal oxygen consumption (VO_{2max}), endospanin-2 Tg mice ran much longer and covered a greater distance than WT or endospanin-1 Tg mice (Figure 5G and Supplemental Figure 8H), while *endospanin-2* $^{-/-}$ mice displayed lower exercise capacity (Figure 5H and Supplemental Figure 8I) and reduced spontaneous locomotor activity in a free wheel exercise compared with their WT littermates (Supplemental Figure 8J). Altogether, these data show that endospanin-2 plays a regulatory role in skeletal muscle metabolic flexibility and function.

Discussion

Dietary energy restriction is a metabolic stress that induces beneficial adaptations of skeletal muscle, resulting in improved health (28). We and others have previously shown that endospanin-1 and endospanin-2 cooperatively control CR-induced metabolic adaptations in the liver by modulating hepatic GH sensitivity (12, 13). In this study, we show that endospanin-2, but not endospanin-1, modulates skeletal muscle function and plasticity. By activating autophagy, endospanin-2 triggers ERK phosphorylation, which leads to decreased mitochondrial ROS production, fast-to-slow fiber-type switch, and enhanced running capacity. Selective AAV-mediated overexpression of endospanin-2 in skeletal muscle reduces oxidative stress and decreases ERK phosphorylation, highlighting that endospanin-2 exerts a direct action in this tissue. Moreover, endospanin-2 Tg mice display increased skeletal muscle glycogen content, increased skeletal muscle insulin sensitivity, and improved glucose homeostasis, suggesting that endospanin-2 promotes skeletal muscle metabolic flexibility to sustain energy production during physical activity. Overall, we show that endospanin-2 overexpression mimicks the beneficial adaptations of skeletal muscle to metabolic challenges (29–32).

CR and/or exercise-mediated antioxidant activities preserve cellular and mitochondrial functions (14). Using both loss- and gain-of-function experiments, we show that endospanin-2 increases oxidative stress resistance, as illustrated by decreased mitochondrial ROS production and increased antioxydant enzyme expression. In line, skeletal muscle UCP3 expression is decreased in endospanin-2 Tg mice, which likely reflects an adaptive response to reduced mitochondrial ROS production (33). Indeed, UCP3 expression is reduced upon endurance training and is negatively correlated with energy efficiency (34).

To decipher the mechanism of action of endospanin-2, which is a tetraspan membrane protein, we assessed signaling pathways of cytosolic-to-mitochondrial signaling. Interestingly, the transient stress induced by resistance exercise activates the ERK pathway (35, 36). Moreover, ERK activation induces fast-to-slow fiber-type transition (27), whereas ERK inhibition decreases slow fiber-type isoforms in vitro (37). Our results demonstrate that overexpression or downregulation of endospanin-2 in vivo and in vitro modulates basal ERK activation. Since in vivo endospanin-2 overexpression is also associated with a fast-to-slow fiber-type switch, higher resistance to fatigue, and enhanced endurance capacity, ERK signaling is

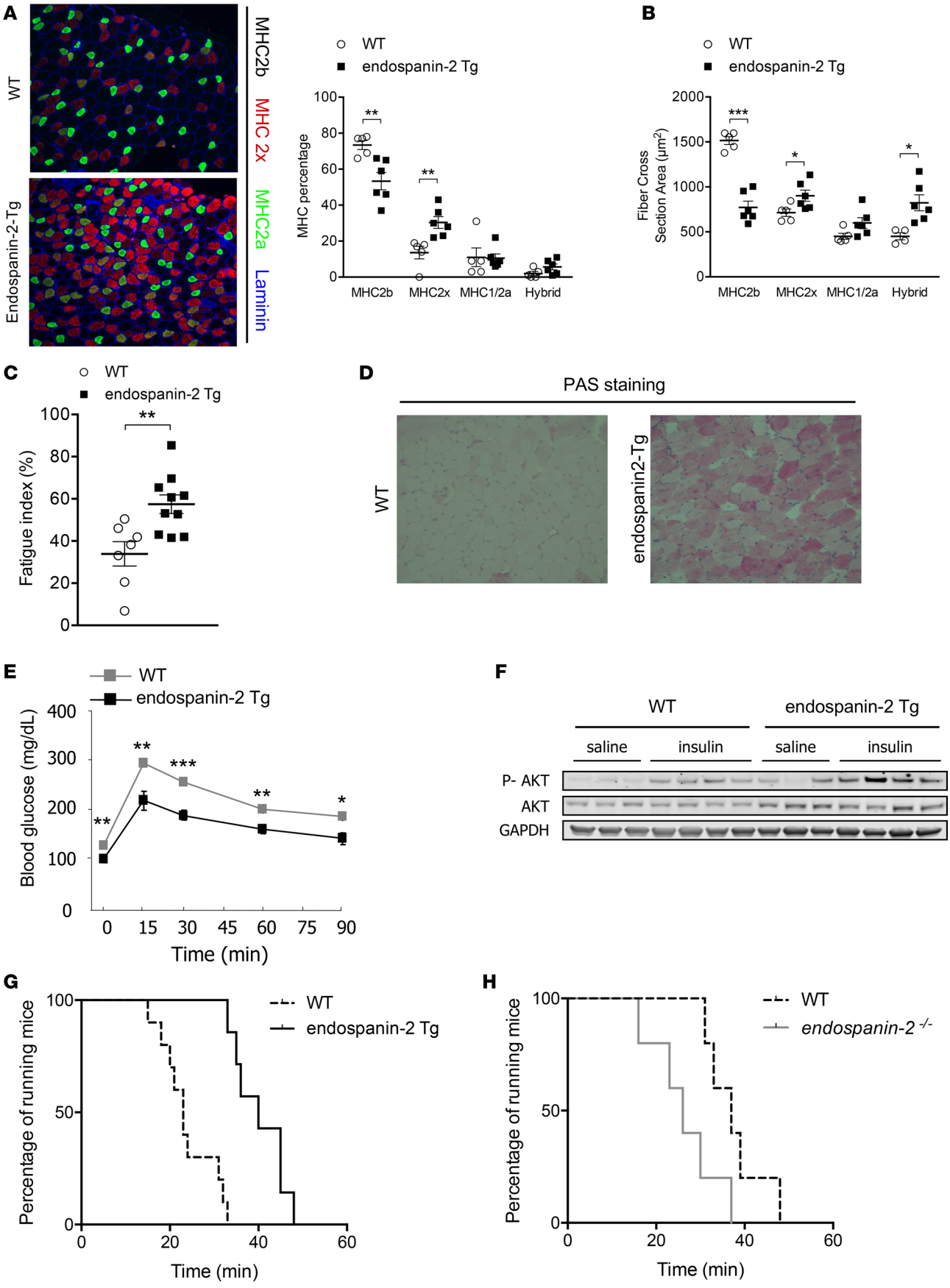
A
WT
Endospanin-2-Tg
MHC2b
MHC 2x
MHC2a
Laminin
WT
endospanin-2 Tg
MHC percentage
MHC2b
MHC2x
MHC1/2a
Hybrid
B
WT
endospanin-2 Tg
Fiber Cross Section Area (μm²)
MHC2b
MHC2x
MHC1/2a
Hybrid
C
WT
endospanin-2 Tg
Fatigue index (%)
D
PAS staining
WT
endospanin2-Tg
E
WT
endospanin-2 Tg
Blood glucose (mg/dL)
Time (min)
F
WT
endospanin-2 Tg
saline
insulin
saline
insulin
P- AKT
AKT
GAPDH
G
WT
endospanin-2 Tg
Percentage of running mice
Time (min)
H
WT
endospanin-2 -/-
Percentage of running mice
Time (min)

Figure 5. Endospanin-2 regulates skeletal muscle plasticity and endurance capacity. (**A**) Representative images of immunofluorescence staining of myosin heavy chain (MHC) and percentage fiber typing of MHC2a (green), MHC2x (red), MHC2b (black), and hybrid (2a and 2x) on EDL sections from endospanin-2 Tg mice compared with their WT littermates (n = 5–6 per genotype). Individual muscle fibers were visualized in blue (laminin staining). (**B**) Evaluation of cross-sectional areas of MHC2b, -2x, -2a, hybrid fibers, and total fiber number of EDL from endospanin-2 Tg mice and their WT littermates (n = 5–6 per genotype). (**C**) Fatigue index evaluated ex vivo on EDL muscle from endospanin-2 Tg mice compared with their WT littermates (n = 8 per genotype). (**D**) Representative images of PAS staining detecting glycogen content on EDL sections from endospanin-2 Tg mice compared with their WT littermates (n = 5–6 per genotype). (**E**) I.p. glucose tolerance test (1 g/kg body weight) of endospanin-2 Tg mice and their WT littermates (n = 6–7 per genotype) (**F**) Western blot analysis of p-AKT and AKT in quadriceps muscle from endospanin-2 Tg mice and their WT littermates under basal and insulin-stimulated conditions (n = 3–4 per genotype) (**G**) Kaplan-Meier curves illustrating the endurance capacity of endospanin-2 Tg mice compared with their WT littermates (n = 7–9 per genotype). (**H**) Kaplan-Meier curves illustrating the endurance capacity of *endospanin-2* $^{-/-}$ mice compared with their WT littermates (n = 5 per genotype).

likely to mediate the endospanin-2–induced skeletal muscle adaptations. Active ERK phosphorylates Stat3 on Serine 727, leading to Stat3 translocation to mitochondria, where it directly modulates the mitochondrial complex I to lower ROS production (20, 38, 39). Increased amounts of total and phosphorylated ERK and total Stat3 were found in skeletal muscle mitochondria from endospanin-2 Tg mice. Moreover, in vitro inhibition of ERK phosphorylation by U0126 reversed the endospanin-2–induced decrease in superoxide production, demonstrating that the reduction in mitochondrial ROS production by endospanin-2 requires activation of the ERK pathway. In addition, mitochondrial localization of ERK is also associated with decreased mitochondrial PTP opening sensitivity (21), which reduces cell susceptibility to apoptosis. Our data show that endospanin-2 reduces mPTP opening susceptibility. Thus, activation of the ERK pathway provides a mechanism through which endospanin-2 initiates a protective response conferring higher resistance to cellular stress associated with decreased mitochondrial ROS production.

Metabolic stress activates autophagy, a highly conserved cell survival process, to minimize damages and to provide energy for short-term survival. This process is essential for dietary restriction and exercise-conveyed skeletal muscle adaptations (22, 23). Indeed, deficiency in skeletal muscle autophagy results in impaired metabolic adaptations to exercise, decreased endurance capacity, and exacerbated age-related skeletal muscle dysfunctions (5, 40). Western blot and electron microscopy analysis of endospanin-2–overexpressing skeletal muscles revealed activated autophagy in glycolytic, but not in oxidative muscle, suggesting that endospanin-2 preserves skeletal muscle function by inducing glycolytic muscle–selective autophagy, a process resembling starvation- and/or exercise-induced autophagy (41). Interestingly, exercise did not further increase autophagy markers in endospanin-2 Tg mice skeletal muscle (data not shown), indicating that endospanin-2 Tg mice display a constitutive increase in autophagy, as observed upon exercise. Moreover, chloroquine treatment delocalizes endospanin-2 from the endosomal compartment to the lysosome, where it colocalizes with LC3-II–positive autophagosomes. Interestingly, autophagic structures serve as cellular platforms promoting ERK phosphorylation (24). Our results show that inhibition of autophagy, either at early or late stages, abolished the altered ERK phosphorylation levels in endospanin-2–overexpressing C2C12 cells, indicating that endospanin-2 regulates ERK phosphorylation levels through autophagy activation. Interestingly, global phosphorylated protein analysis in yeast found a physical interaction between Vps55 (the endospanins yeast homologue) and the serine/threonine kinase ATG1 (the Ulk1 yeast homologue), a key protein involved in the initiation of autophagy following starvation (42). Moreover, Vps55 mutants display decreased oxidative and chemical stress resistance (43), as well as decreased sporulation capacity in response to starvation (44). Altogether, our results indicate that endospanin-2, by modulating autophagosome trafficking to the lysosome, activates autophagy and triggers ERK phosphorylation to increase cellular stress resistance.

In conclusion, our data show that endospanin-2 expression is induced in skeletal muscle during CR and that endospanin-2 overexpression, by activating autophagy-mediated ERK phosphorylation, decreases mitochondrial oxidative stress and modulates skeletal muscle function. This study supports a prominent role of endospanin-2 in skeletal muscle plasticity and metabolic flexibility, resulting in enhanced running capacity.

Methods

Supplemental Methods are available online with this article.

Mice. We used Tg human endospanin-1 and endospanin-2 male mice on a C57Bl/6 background, which overexpress human endospanin-1 (or LEPROT) and endospanin-2 (or LEPROTL1) in all tissues, including skeletal muscle, as previously described (12). *Endospanin-2*–KO (or *Leprotl1*) mice were generated using

leprotl1$^{tm1a(EUCOMM)hmgu}$ ES cells (European Conditional Mouse Mutagenesis). Mice were backcrossed with C57BL/6J for 10 generations, and heterozygotes were inbred (see Supplemental informations). Male and female mice were used at 15–20 weeks of age. All mice were housed in a 12-hour/12-hour light/dark cycle, and the *ad libitum*–fed (AL-fed) group had free access to water and regular chow diet (A03; Usine d'Alimentation Rationelle), but CR mice were fed at 70% of the food intake of their AL-fed littermates during 4 weeks.

Cell culture. Mouse C2C12 myoblasts (CRL-1772, American Type Culture Collection) were cultured in DMEM (4.5 g/l D Glucose; Gibco) supplemented with 10% FBS and 1% gentamycin at 37°C and 5% CO_2. C2C12 cells allowed to reach 90% of confluence were differentiated into myotubes by adding DMEM supplemented with 2% horse serum (HS) during 5 days. Cell lines constitutively overexpressing endospanin-1 and endospanin-2 were generated as previously described (45). Endospanin-1 and endospanin-2 overexpression was verified by quantitative PCR (qPCR) and Western blot on endospanin-1 and endospanin-2 C2C12 cells compared with pBabe control cells. For autophagy experiments, cells were cultured in HBSS and either treated with wortmannin (Merck, 100 nM) or chloroquine (Merck, 50 μM) or their respective vehicle for 4 hours.

Mitochondrial ROS production in plasma and isolated mitochondria. H_2O_2 production from plasma and skeletal muscle mitochondria was measured fluorimetrically using Amplex Red (Molecular Probes, Invitrogen). Mitochondria (30 μg of mitochondrial proteins/well) were incubated in mitochondrial respiration medium (Mir05) in the presence of the respiratory chain complex II substrate succinate (Merck, 10 mM), with or without complex I and III inhibitors — i.e., rotenone (Merck, 1 μM) and antimycin A (Merck, 2.5 μM), respectively. Reactions were set up in triplicate in the presence of 50 μM of Amplex Red and 0.1 unit/ml horseradish peroxidase in a 96-well plate. Fluorescence (excitation wavelength λ_{ex}=545 nm, emission wavelength λ_{em}=590 nm) was kinetically followed during 30 minutes at 37°C, using a Tecan Infinite F500 apparatus (Tecan Systems). For quantification, 2 wells containing 10 μM H_2O_2 were added on each plate. All results were expressed in nmol of produced H_2O_2 per mg of mitochondrial proteins per minute.

Mitochondrial swelling assay. Mitochondrial swelling consecutive to PTP opening was monitored by the decrease of 90° light scatter at 540 nm in a spectrophotometer as described (46). Briefly, a mitochondrial pellet was suspended in swelling buffer (0.4 mg/ml), and 200 μl/well was added in a 96-well plate. A PTP opening was induced by the addition of 75 μM Ca^{2+}.

MHC immunofluorescence. Conventional immunofluorescence for MHC subtyping was performed on transverse cryosections of EDL and Soleus muscle. MHC2a, visualized in green, was stained using a monoclonal antibody (N2.261, Developmental Studies Hybridoma Bank) directed against human neonatal MHC human neonatal slow type 1 and type 2a. MHC2x, visualized in red, was stained using a mouse IgM polyclonal antibody directed against rabbit MHC type 2x (6H1, Developmental Studies Hybridoma Bank). Individual muscle fibers were visualized using a primary antibody against the basement membrane marker laminin (rabbit polyclonal antibody, L-9393, Merck), which was visualized in blue. The following secondary antibodies were used: for the myosin 1/2a a goat anti–mouse IgG1 AlexaFluor 488 (A-21121, Thermo Fisher Scientific), for the myosin 2x a goat anti–mouse IgM AlexaFLuor 555 (A-21426, Thermo Fisher Scientific), for the laminin a goat anti–rabbit IgG AlexaFluor 350 (A-11069, Thermo Fisher Scientific).

Maximal exercise stress test and endurance capacity. Mice were acclimated to the treadmill by performing a 10 m/min run 2 days prior to the experiment. The day of the exercise stress test, mice were placed onto the treadmill enclosed in a metabolic chamber connected to an O_2 sensor (Oxymax, Columbus Instruments). Basal VO_2 (VO_{2b}) was measured after a 30-minute resting period, and then mice started running at 10 m/min in a 0% incline. Speed was incremented by 4 m/min every 3 minutes until exhaustion in order to determine their VO_{2max}. Exhaustion was reached when mice remained on the electrical shocker plate for 5 seconds. Speed corresponding to VO_{2max} was determined and considered as the maximal running speed (v_{max}). Two days later, mice ran at a speed equivalent to 70% of their v_{max} until exhaustion in order to determine their maximal endurance capacity. Time to exhaustion and total run distance were determined.

Daily wheel-running activity. To analyze daily wheel-running activity, mice were placed into individual cages containing running wheels for 1 week (Campden, Phymep). Wheel revolution was recorded daily and averaged.

Statistics. Values are means ± SEM of the indicated number of measurements. Statistical significance was determined using 2-tailed unpaired Student's *t* test or 1-way ANOVA with $P < 0.05$.

Study approval. Experimental protocols were performed with the approval of the Nord Pas de Calais ethics committee (CEEA75) and in compliance with French and European ethical legislations.

Author contributions

SL, YS, BS, and B. Bailleul were responsible for the study design, data analysis, and interpretation of data, and they cowrote the manuscript; YS, SL, MKCH, EW, FP, QT, AML, BP, OB, YR, HD, and B. Bastide performed the experiments and data analysis; ED, SD, CD, QT, VM, NB, and GS gave technical and material support; JPS, PS, and B. Bailleul were involved in data analysis. All authors have discussed the results, commented on the manuscript, and approved the final manuscript.

Acknowledgments

This research was supported by the European Genomic Institute for Diabetes (EGID, ANR-10-LABX-46) and European Commission, Lille Métropole Communauté Urbaine (to YS), Région Nord Pas-de-Calais/FEDER (to BS), CPER 2011-R3-P12A (to B. Bailleul), a joint Société Francophone du Diabète (SFD)/Menarini research fellowship (to B. Bailleul), EFSD/Lilly research grant and CPER emerging team (to HD), Eurhythdia (to BS and HD), ERC Région Haut de France (to HD), and Pfizer France and Ipsen Beaufour (to JPS). BS hold an ERC advanced grant (no. 694717).

Address correspondence to: Yasmine Sebti or Bart Staels, UMR1011 INSERM, Institut Pasteur de Lille, BP 245, 1, rue Calmette, 59019 Lille, France. Phone: 33.3.20.87.71.25; Email: yasmine.sebti@pasteur-lille.fr (YS). Phone: 33.3.20.87.73.88; Email: Bart.Staels@pasteur-lille.fr (BS).

1. Hoeks J, Schrauwen P. Muscle mitochondria and insulin resistance: a human perspective. *Trends Endocrinol Metab*. 2012;23(9):444–450.
2. Szendroedi J, Phielix E, Roden M. The role of mitochondria in insulin resistance and type 2 diabetes mellitus. *Nat Rev Endocrinol*. 2011;8(2):92–103.
3. Lass A, Sohal BH, Weindruch R, Forster MJ, Sohal RS. Caloric restriction prevents age-associated accrual of oxidative damage to mouse skeletal muscle mitochondria. *Free Radic Biol Med*. 1998;25(9):1089–1097.
4. Jia K, Levine B. Autophagy is required for dietary restriction-mediated life span extension in C. elegans. *Autophagy*. 2007;3(6):597–599.
5. Lira VA, et al. Autophagy is required for exercise training-induced skeletal muscle adaptation and improvement of physical performance. *FASEB J*. 2013;27(10):4184–4193.
6. Rubinsztein DC, Mariño G, Kroemer G. Autophagy and aging. *Cell*. 2011;146(5):682–695.
7. Bailleul B, Akerblom I, Strosberg AD. The leptin receptor promoter controls expression of a second distinct protein. *Nucleic Acids Res*. 1997;25(14):2752–2758.
8. Huang Y, et al. Cloning and characterization of a novel human leptin receptor overlapping transcript-like 1 gene (LEPROTL1). *Biochim Biophys Acta*. 2001;1517(2):327–331.
9. Belgareh-Touzé N, Avaro S, Rouillé Y, Hoflack B, Haguenauer-Tsapis R. Yeast Vps55p, a functional homolog of human obesity receptor gene-related protein, is involved in late endosome to vacuole trafficking. *Mol Biol Cell*. 2002;13(5):1694–1708.
10. Couturier C, et al. Silencing of OB-RGRP in mouse hypothalamic arcuate nucleus increases leptin receptor signaling and prevents diet-induced obesity. *Proc Natl Acad Sci USA*. 2007;104(49):19476–19481.
11. Séron K, et al. Endospanins regulate a postinternalization step of the leptin receptor endocytic pathway. *J Biol Chem*. 2011;286(20):17968–17981.
12. Touvier T, et al. LEPROT and LEPROTL1 cooperatively decrease hepatic growth hormone action in mice. *J Clin Invest*. 2009;119(12):3830–3838.
13. Wu S, Grunwald T, Kharitonenkov A, Dam J, Jockers R, De Luca F. Increased expression of fibroblast growth factor 21 (FGF21) during chronic undernutrition causes growth hormone insensitivity in chondrocytes by inducing leptin receptor overlapping transcript (LEPROT) and leptin receptor overlapping transcript-like 1 (LEPROTL1) expression. *J Biol Chem*. 2013;288(38):27375–27383.
14. Lanza IR, et al. Chronic caloric restriction preserves mitochondrial function in senescence without increasing mitochondrial biogenesis. *Cell Metab*. 2012;16(6):777–788.
15. Robinson KM, Janes MS, Beckman JS. The selective detection of mitochondrial superoxide by live cell imaging. *Nat Protoc*. 2008;3(6):941–947.
16. Alonso M, et al. Mitochondrial extracellular signal-regulated kinases 1/2 (ERK1/2) are modulated during brain development. *J Neurochem*. 2004;89(1):248–256.
17. Baines CP, et al. Mitochondrial PKCepsilon and MAPK form signaling modules in the murine heart: enhanced mitochondrial PKCepsilon-MAPK interactions and differential MAPK activation in PKCepsilon-induced cardioprotection. *Circ Res*. 2002;90(4):390–397.
18. Chung J, Uchida E, Grammer TC, Blenis J. STAT3 serine phosphorylation by ERK-dependent and -independent pathways negatively modulates its tyrosine phosphorylation. *Mol Cell Biol*. 1997;17(11):6508–6516.
19. Gough DJ, Koetz L, Levy DE. The MEK-ERK pathway is necessary for serine phosphorylation of mitochondrial STAT3 and Ras-mediated transformation. *PLoS ONE*. 2013;8(11):e83395.
20. Szczepanek K, et al. Mitochondrial-targeted Signal transducer and activator of transcription 3 (STAT3) protects against ischemia-induced changes in the electron transport chain and the generation of reactive oxygen species. *J Biol Chem*. 2011;286(34):29610–29620.

21. Rasola A, Sciacovelli M, Chiara F, Pantic B, Brusilow WS, Bernardi P. Activation of mitochondrial ERK protects cancer cells from death through inhibition of the permeability transition. *Proc Natl Acad Sci USA*. 2010;107(2):726–731.
22. Morselli E, et al. Caloric restriction and resveratrol promote longevity through the Sirtuin-1-dependent induction of autophagy. *Cell Death Dis*. 2010;1:e10.
23. He C, et al. Exercise-induced BCL2-regulated autophagy is required for muscle glucose homeostasis. *Nature*. 2012;481(7382):511–515.
24. Martinez-Lopez N, Athonvarangkul D, Mishall P, Sahu S, Singh R. Autophagy proteins regulate ERK phosphorylation. *Nat Commun*. 2013;4:2799.
25. Lecarpentier Y. Physiological role of free radicals in skeletal muscles. *J Appl Physiol*. 2007;103(6):1917–1918.
26. Dupont E, Cieniewski-Bernard C, Bastide B, Stevens L. Electrostimulation during hindlimb unloading modulates PI3K-AKT downstream targets without preventing soleus atrophy and restores slow phenotype through ERK. *Am J Physiol Regul Integr Comp Physiol*. 2011;300(2):R408–R417.
27. Murgia M, Serrano AL, Calabria E, Pallafacchina G, Lomo T, Schiaffino S. Ras is involved in nerve-activity-dependent regulation of muscle genes. *Nat Cell Biol*. 2000;2(3):142–147.
28. Gaman L, Stoian I, Atanasiu V. Can aging be slowed?: Hormetic and redox perspectives. *J Med Life*. 2011;4(4):346–351.
29. Allen DL, Harrison BC, Maass A, Bell ML, Byrnes WC, Leinwand LA. Cardiac and skeletal muscle adaptations to voluntary wheel running in the mouse. *J Appl Physiol*. 2001;90(5):1900–1908.
30. Chen D, Steele AD, Lindquist S, Guarente L. Increase in activity during calorie restriction requires Sirt1. *Science*. 2005;310(5754):1641.
31. de Lange P, et al. Sequential changes in the signal transduction responses of skeletal muscle following food deprivation. *FASEB J*. 2006;20(14):2579–2581.
32. Manabe Y, et al. Exercise training-induced adaptations associated with increases in skeletal muscle glycogen content. *FEBS J*. 2013;280(3):916–926.
33. Echtay KS, et al. Superoxide activates mitochondrial uncoupling proteins. *Nature*. 2002;415(6867):96–99.
34. Schrauwen P, Hesselink M. Uncoupling protein 3 and physical activity: the role of uncoupling protein 3 in energy metabolism revisited. *Proc Nutr Soc*. 2003;62(3):635–643.
35. Goodyear LJ, Chang PY, Sherwood DJ, Dufresne SD, Moller DE. Effects of exercise and insulin on mitogen-activated protein kinase signaling pathways in rat skeletal muscle. *Am J Physiol*. 1996;271(2 Pt 1):E403–E408.
36. Kramer HF, Goodyear LJ. Exercise, MAPK, and NF-kappaB signaling in skeletal muscle. *J Appl Physiol*. 2007;103(1):388–395.
37. Higginson J, et al. Blockades of mitogen-activated protein kinase and calcineurin both change fibre-type markers in skeletal muscle culture. *Pflugers Arch*. 2002;445(3):437–443.
38. Sarafian TA, et al. Disruption of astrocyte STAT3 signaling decreases mitochondrial function and increases oxidative stress in vitro. *PLoS ONE*. 2010;5(3):e9532.
39. Szczepanek K, Chen Q, Larner AC, Lesnefsky EJ. Cytoprotection by the modulation of mitochondrial electron transport chain: the emerging role of mitochondrial STAT3. *Mitochondrion*. 2012;12(2):180–189.
40. Carnio S, et al. Autophagy impairment in muscle induces neuromuscular junction degeneration and precocious aging. *Cell Rep*. 2014;8(5):1509–1521.
41. Ogata T, Oishi Y, Higuchi M, Muraoka I. Fasting-related autophagic response in slow- and fast-twitch skeletal muscle. *Biochem Biophys Res Commun*. 2010;394(1):136–140.
42. Ptacek J, et al. Global analysis of protein phosphorylation in yeast. *Nature*. 2005;438(7068):679–684.
43. Higgins VJ, Alic N, Thorpe GW, Breitenbach M, Larsson V, Dawes IW. Phenotypic analysis of gene deletant strains for sensitivity to oxidative stress. *Yeast*. 2002;19(3):203–214.
44. Deutschbauer AM, Williams RM, Chu AM, Davis RW. Parallel phenotypic analysis of sporulation and postgermination growth in Saccharomyces cerevisiae. *Proc Natl Acad Sci USA*. 2002;99(24):15530–15535.
45. Woldt E, et al. Rev-erb-α modulates skeletal muscle oxidative capacity by regulating mitochondrial biogenesis and autophagy. *Nat Med*. 2013;19(8):1039–1046.
46. Zamzami N, Maisse C, Métivier D, Kroemer G. Measurement of membrane permeability and the permeability transition of mitochondria. *Methods Cell Biol*. 2007;80:327–340.